Micromachining of polyurea aerogel using femtosecond laser pulses

Qiumei Bian [a,*], Shouyuan Chen [a], Byung-Tai Kim [b], Nicholas Leventis [c], Hongbing Lu [d],
Zenghu Chang [a], Shuting Lei [a]

[a] Kansas State University, USA
[b] Cheongju University, Republic of Korea
[c] Missouri University of Science and Technology, USA
[d] The University of Texas at Dallas, USA

ARTICLE INFO

ABSTRACT

We successfully sliced cylindrical polyurea aerogel samples of 10–15 mm in diameter into 1–3 mm disks using femtosecond laser. The experiments were performed using a Ti:sapphire laser with 800 nm wavelength in ambient air with a pulse duration of ~40 fs. We found that the laser fluence to breakdown this material is 1.3 J/cm^2. The ablation rate at different energy levels was evaluated. The factors influencing the ablation surface quality were investigated. The proper fluence to slice the porous polyurea is 6.4–8.9 J/cm^2 with the beam linearly scanning the sample at a speed of 0.1 mm/s, or 5.1–7.6 J/cm^2 with the beam circularly scanning the sample at a speed of 3.5–4°/s, and high quality machining surface was obtained under these conditions. The material removal mechanisms are proposed. Structural details of the machined area were characterized using a number of techniques such as optical microscopy and scanning electron microscopy. This work provides insights for micromachining nanostructured porous polymers using femtosecond lasers.

1. Introduction

The excellent mechanical and thermal properties, combined with their unique porous structure, have made polyurea aerogels very attractive for many potential applications including lightweight thermal and acoustic insulations, radiation shielding, and vibration damping [1,2]. Consequently, considerable efforts have been made to fabricate the nanostructured porous materials for various applications. However, it is difficult to cut these materials using traditional machining operations such as cutting, milling, and grinding due to their soft and porous nanoscale structures [2,3]. The recommended tool for cutting the aerogels is a diamond saw [2]. However machining using traditional approaches will introduce damage to the surface and induce collapse of porous structures near the finished surface that could alter a suite of excellent properties derived from the porous nanostructures. How to process the aerogels to achieve good surface finish remains a challenge.

Ultra high intensity femtosecond laser has been explored extensively as a potentially fast and economical tool for micro/nanomachining of various materials. Advantages using femtosecond laser for machining include high precision with negligible collateral damages, no restrictions to material type, and machining in the bulk [4]. Hence, femtosecond laser micromachining provides an alternative method to cut polymers due to its non-contact nature of material removal. In recent years, femtosecond laser micromachining has been developed to ablate microscale features in many materials including polymers [4,5,11,12,18]. For example, femtosecond laser micromachining has been used to fabricate miniature devices using polymer materials including polyethylene [6] and silicone-based hydrogel polymers [7]. Also, ultrafast laser micromachining of silica aerogel has been reported [8]. Several operating factors that affect the micromachining process have been investigated, such as the linear transmission of laser light and the material breakdown threshold fluence of the silica aerogels [8]. Meanwhile, femtosecond laser ablation of polytetrafluoroethylene has been investigated [9], and the experimental results indicate that a sufficiently large pulse number and the control of laser intensity are two key factors in obtaining high quality microstructures.

In addition, the mechanism of light–matter interaction especially the ultrafast laser pulse–matter interaction is fundamentally important [13]. Femtosecond laser ablation mechanism of polymers has been reported by Reyna and coworkers. And a photo-thermal model was presented in their paper [10]. However, there are only few studies in laser processing of polyurea aerogels to the best of our knowledge. The interaction between the laser pulse and the porous polymer needs further investigation. It is also vital to determine the right combination of laser ablation parameters in order to obtain the desired shape with good surface quality. To achieve this, appropriate settings of laser intensity, pulse number and pulse duration as well as their ratio are critical [12].

* Corresponding author.
  E-mail address: bian@ksu.edu (Q. Bian).

In this paper, we report femtosecond laser micromachining of polyurea aerogels in ambient air using a Ti:sapphire laser with 800 nm wavelength and 40 fs pulse duration, and also propose mechanisms for material removal.

2. Experimental aspects

2.1. Experimental setup

A schematic diagram of the experimental setup for femtosecond laser micromachining system is given in Fig. 1. The femtosecond laser pulses were generated using a Ti:sapphire laser system, which could produce pulses with ~40 fs duration and at 800 nm center wavelength. The repetition rate was 1 kHz and the maximum pulse energy was 6 mJ. The laser beam diameter was 10 mm and the M^2 of the laser beam was 1.35. After passing a 50–50 beam splitter, a neutral density filter was used to adjust the laser pulse energy. A quarter-wave plate was used to generate a circularly polarized laser beam. The laser beam was focused by a lens with 500 mm focal length. It was focused at the center of the sample. The sample was mounted on a computer controlled micro-positioning stage so that the sample could be rotated or translated in 3D. All the experiments were conducted in ambient air at atmospheric pressure and room temperature (near 25 °C). After machining, the samples were analyzed using an optical microscope and a scanning electron microscope (SEM).

2.2. Sample preparation

Polyurea aerogels of different densities were prepared by varying the concentration of Desmodur N3300A (courtesy of Bayer Corp) in the sol according to a modification of a process developed by Leventis [19]. Typically, low-density (0.016 g/cm^3) polyurea aerogels were prepared by mixing 5.5 g (0.0109 mol) of N3300A (1,3,5-tris(6-isocyanatohexyl)-1,3,5-triazinane-2,4,6-trione) in 94 ml of dry acetone, 1.5 equivalents of water (0.2945 ml, 0.01635 mol) relative to the mol of N3300A in the sol and 0.327 ml triethylamine (ACROS, 99% pure, distilled, 0.3% w/w relative to the total weight of Desmodur N3300A plus solvent used in the sol). The resulting sol was shaken vigorously and was poured into polyethylene syringe molds and its gelation time was found to be 8 h. Higher-density (0.55 g/cm^3) polyurea aerogels were prepared by increasing the concentration of N3300A in the sol. Two types of high-density polyurea aerogels were prepared, one with 11 g (0.02108 mol) of N3300 A in 94 ml of dry acetone and another with 16.5 g (0.0327 mol) of N3300A in 94 ml of distilled acetone, by adding 1.5 equivalents of water relative to the mol of N3300A and 0.351 ml of TEA for 11 g of N3300 A and 0.375 ml of TEA for 16.5 g of N3300 A, and the gelation time was found to be 4 h and 2 h, respectively. After aging for a day both the low-density and high-density polyurea wet gels were washed with acetone, approximately 4 times the volume of the gel. The solvent was exchanged 2 times once every 24 h. Finally the wet gels were dried supercritically.
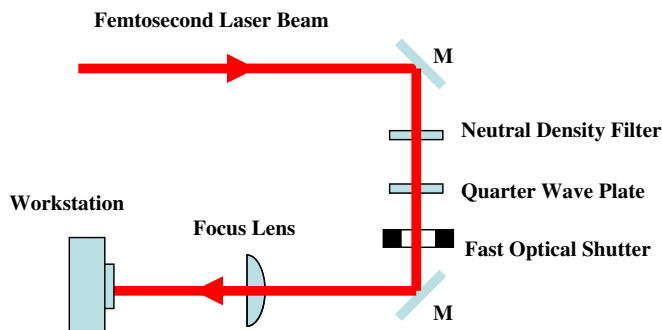
The gelation time was found to vary with respect to the amount of catalyst and the amount of water added to the sol. Fig. 2 shows a high-density polyurea aerogel sample and its microstructure. The material shows hierarchical structures including an assembly of nanoparticles at the microscale. It is highly porous with a porosity of ~85% and a mass density of ~0.2 g/cm^3.

In this study, at first laser ablation experiments were conducted to determine the material breakdown threshold and ablation rate. To this end, laser pulse number was controlled using a fast electronic shutter. The shutter had a 6 mm aperture and 150 Hz frequency at continual operation mode. Also, the surface quality was investigated, together with the effect of the pulse energy and the sample scanning speed. The influence of the incident pulse energy and the sample scanning speed on the surface quality was investigated separately. The average laser power was measured by the portable laser power meter with ±1% accuracy and 3 mW to 10 W measurement ranges. It was measured before the focusing lens. The experiments to determine suitable cutting conditions were conducted in two different ways: a) a sample was mounted on the linear translation stage and the beam cut through the entire sample and sliced it off, as shown in Fig. 3(a); b) a sample was mounted on the rotating stage and the sample rotated around its own axis while the laser beam pointed towards the center of the sample at normal incidence, as shown in Fig. 3(b).

3. Results

3.1. Material breakdown threshold and ablation rate

Material breakdown threshold is a characteristic depending on the laser wavelength, pulse duration, repetition rate and number of laser shots. It is ideally defined as the energy fluence at which irreversible damage occurs in the material by removing a monolayer of material. It is usually determined by visual examination, ablation depth measurement, plasma radiation monitoring, etc. In this work, the material breakdown threshold was estimated using the following linear relationship between the square of the crater diameter and the logarithm of the laser fluence or energy [15,20]:

$$D^2 = 2w_0^2 \ln(F_0 / F_{th}) \text{ or } D^2 = 2w_0^2 \ln(E_0 / E_{th}) \qquad (1)$$

where D is the diameter of the ablated spots after ten shots, F_{th} is ablation threshold fluence, F_0 is applied laser fluence, E_{th} is ablation threshold energy, E_0 is applied laser energy, and $2w_0$ is focal spot size. The diameter of the ablated spots was measured from the profiles obtained with optical micrographs. To determine the random errors of the crater diameter, we repeated the experiments and measurements three times under each given set of conditions. We obtained the average value of the crater diameter and found that the maximum error was 7%. A plot of the square of damage diameter, D^2, as a function of the logarithm of laser fluence is shown in Fig. 4. The error bars indicate the maximum error of each data point. A linear fit was made to the experimental data. The slope of the line is two times the square of the spot size and the intercept of the extrapolated line with the horizontal axis is the ablation threshold. The spot size was found to be 115 μm and the ablation threshold was 1.3 J/cm^2 for the 40 fs pulse duration and 800 nm center wavelength. The spot size was slightly different from the value of 105 μm measured by a CCD camera because the pulse number in our experiment was ten instead of one. With the increase of pulse number, the ablated craters became greater, resulting in a focal spot size that was slightly larger than the results measured by the CCD camera. In comparison, the ablation thresholds of two solid polymers PMMA and PC at 800 nm, 150 fs duration and 10 pulses were 1.5 J/cm^2 and 1.1 J/cm^2, respectively [20]. The slightly higher threshold for polyurea aerogel compared to these two polymers is because the femtosecond laser ablation depends strongly on the type, dimensions and distribution of the filling
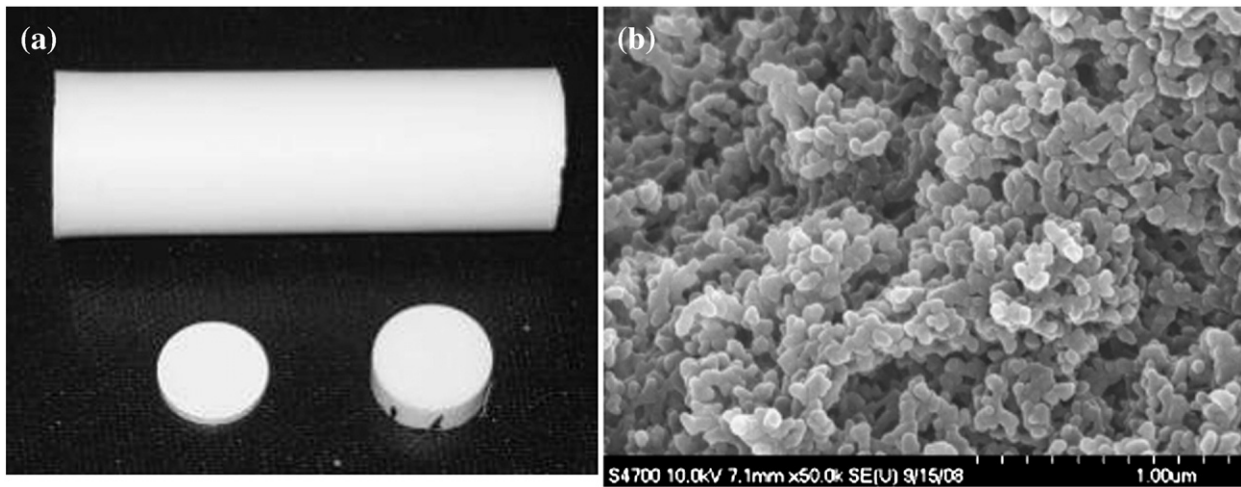

Fig. 1. Schematic of the experimental setup.

Fig. 2. High-density polyurea aerogel sample: (a) optical image of a cylindrical sample of 13 mm in diameter (b) SEM image of the porous polyurea particulate microstructure.

material within the polymer matrix according to Moreno and coworkers [17].

The average ablation rate was determined by measuring the depth of the ablated hole at 1000 and 5000 shots, as shown in Fig. 5. The depth and diameter of the ablated holes and grooves were measured from profiles captured by scanning electron micrographs and optical micrographs. In order to observe the depth of the hole, we cut the sample through the center line of the hole and observed the cross section of the hole. In or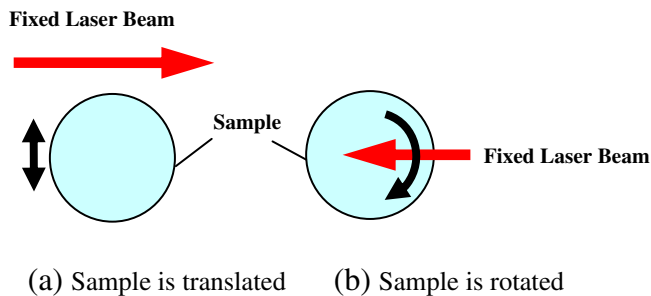der to determine the random errors, we repeated the experiments and measurements three times under each given set of conditions. We obtained the average value of the hole depth and found that the maximum error was 6.5%. In comparison with PMMA and PC the ablation rate is higher at the same energy level because of the high porosity (85%) of the polyurea aerogel in air [20]. Most of the time, the beam propagated in air instead of interacting with the material. It is seen from Fig. 5 that the average ablation rate at 1000 pulses is much higher than at 5000 shots for the same energy level. The difference could be attributed mainly to the following two factors. One is that the beam becomes more diverged after the depth is beyond the Rayleigh range according to the Gaussian beam property [9]. The other reason is because of the energy loss due to light scattering and dispersion, which becomes significant with the increase of depth in the porous material. Beam scattering and dispersion were noticeable by making the surrounding materials glow during the ablation process. Both factors make the beam intensity to decrease rapidly, resulting in the reduction of the average ablation rate because the subsequent pulses lose the ability to efficiently remove the material.

3.2. Surface morphology and quality

The periodic groove structure was observed on the ablated surfaces as shown in Fig. 6. Fig. 6 (a) shows the cutting surface with the sample linearly translating through the beam (the laser beam

Fig. 3. Schematic illustration of the cutting methods: (a) sample mounted on 3D translation stage (b) sample mounted on rotary stage.

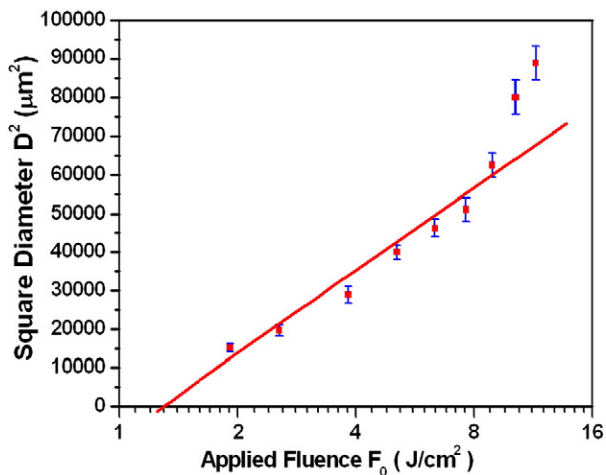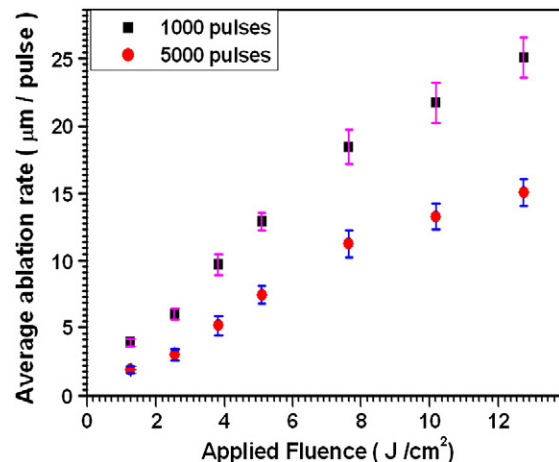**Fig. 4.** D^2 of the modified area versus pulse fluence.

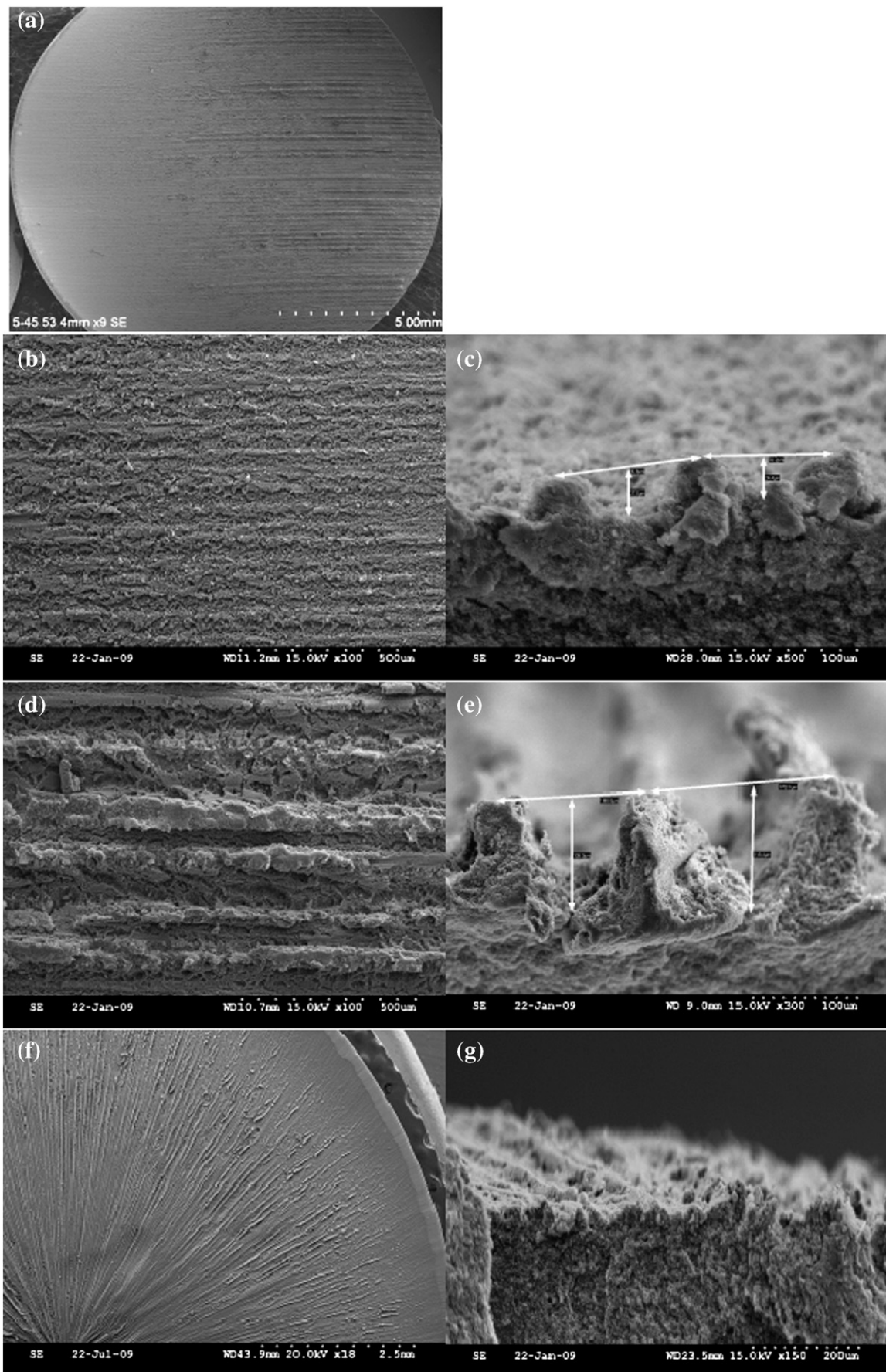**Fig. 5.** Average ablation rate versus pulse fluence.

Fig. 6. SEM images of typical cutting surfaces of polyurea aerogel: (a) linear scanning speed of 0.1 mm/s and laser fluence of 6.36 J/cm² (b) beam incident side of (a) (c) cross-section of incident side (d) beam exit side of (a) (e) cross-section of exit side (f) circular scanning speed of 4 degree/s and fluence of 5.1 J/cm² (g) cross section of (f) at 2 mm from the edge.
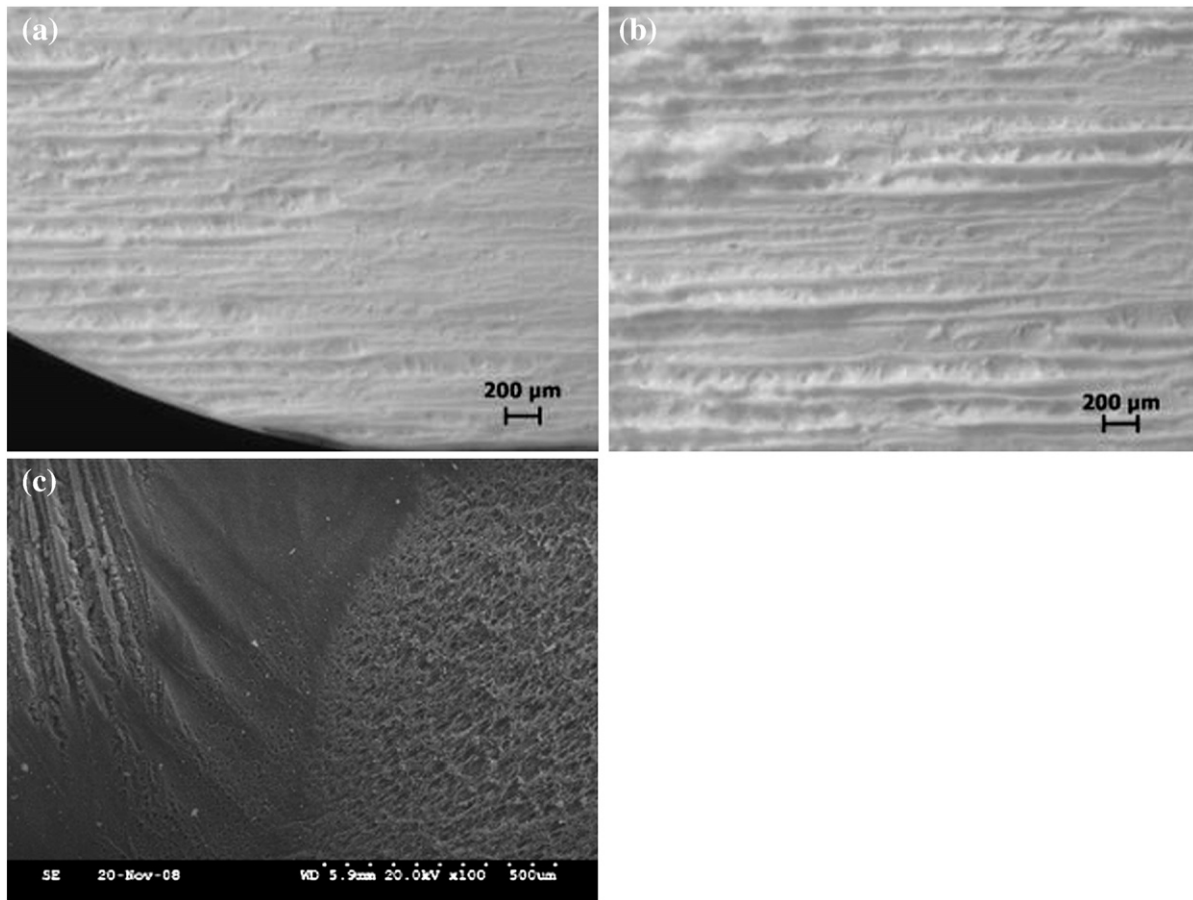
Fig. 7. Images of cut surfaces showing the dependence of groove width and depth on the scanning speed at fluence of 6.3 J/cm^2: (a) scanning speed at 0.05 mm/s (b) scanning speed at 0.2 mm/s (c) scanning speed at 0.02 mm/s.

propagates from left to right and the sample moves orthogonal to the beam). The scanning speed was 0.1 mm/s and the laser fluence was 6.36 J/cm^2. It is seen that the surface quality varies from the beam incident side to the beam exit side. The surface quality at the beam incident side (left side of Fig. 6 (a)) is much better than that at the beam exit side (right side of Fig. 6 (a)). SEM examination reveals that the incident side of the sample has small groove width, which is clearly visible in Fig. 6 (a), (b), and (c). The images indicate that at the incident side groove width and depth are about 80 μm and 30 μm, respectively, which are smaller than the corresponding values at the exit side, which are about 280 μm and 140 μm, respectively, as shown in Fig. 6 (a), (d), and (e).

To improve the cutting surface quality we reduced the beam traveling distance in the material by mounting the sample on a rotation stage with the beam circularly scanning the sample so that the path of the beam interaction with the material was reduced to half comparing with the linear scan. Laser beam was directed to the center of the sample. The scanning speed was 4 degree/s and the laser fluence was 5.1 J/cm^2. In this way a smaller surface roughness was achieved, as shown in Fig. 6 (f) and (g). It is seen that the groove width and depth are improved to less than the focal spot size at the center of the sample, which is much better than the results when the beam linearly scanned the sample. However, the grooves are distributed radially towards the sample center instead of parallel to each other.

Besides the beam propagation distance in the material, the other key factors affecting the quality of the cutting surface are the sample scanning speed and the laser fluence. We studied the influence of them on the ablated surface quality in two separated sets of experiments. The beam spot size on the sample surface was 107 μm,

measured using CCD camera. It was fixed because a long Rayleigh range was required to slice a cylindrical sample of more than 13 mm in diameter. A long Rayleigh range is associated with a large focal spot size; therefore, the final focus lens and focal spot size of 107 μm were the results of the desired Rayleigh range. In the process of surface cutting, the sample was exposed to multiple pulses while being continuously translated at the scanning speed. It is convenient to relate the scanning speed to an effective pulse number delivered in order to compare the results to the stationary process. The approximate relation that accounts for the effective pulse number incident over the distance of the beam spot size is given by

$$N = RS / V \tag{2}$$

where N is the pulse number, R is the pulse repetition rate, S is the beam diameter and V is the sample scanning speed [9]. The expression can be used to calculate the accumulated fluence of a series of pulses with a Gaussian intensity profile, peak fluence of φ_o and separated by V/R, the distance traveled between pulses. It is noteworthy to point out that this is an approximate relation and is not expected to be completely equivalent to stationary processing with N pulses. Nevertheless it is instructive in a first analysis of the surface cutting results. In the subsequent discussions, all the references to the number of pulses are based on the conversion of the scanning speed V to the number of pulses N in Eq. (2).

In the first set of experiments, the pulse energy (fluence) was held constant at $E_0 = 0.5$ mJ ($\varphi_0 = 6.3$ J/cm^2) and the dependence of the surface quality on the scanning speed was investigated in the range of V = 0.02 mm/s–0.2 mm/s (N = 5000–500).
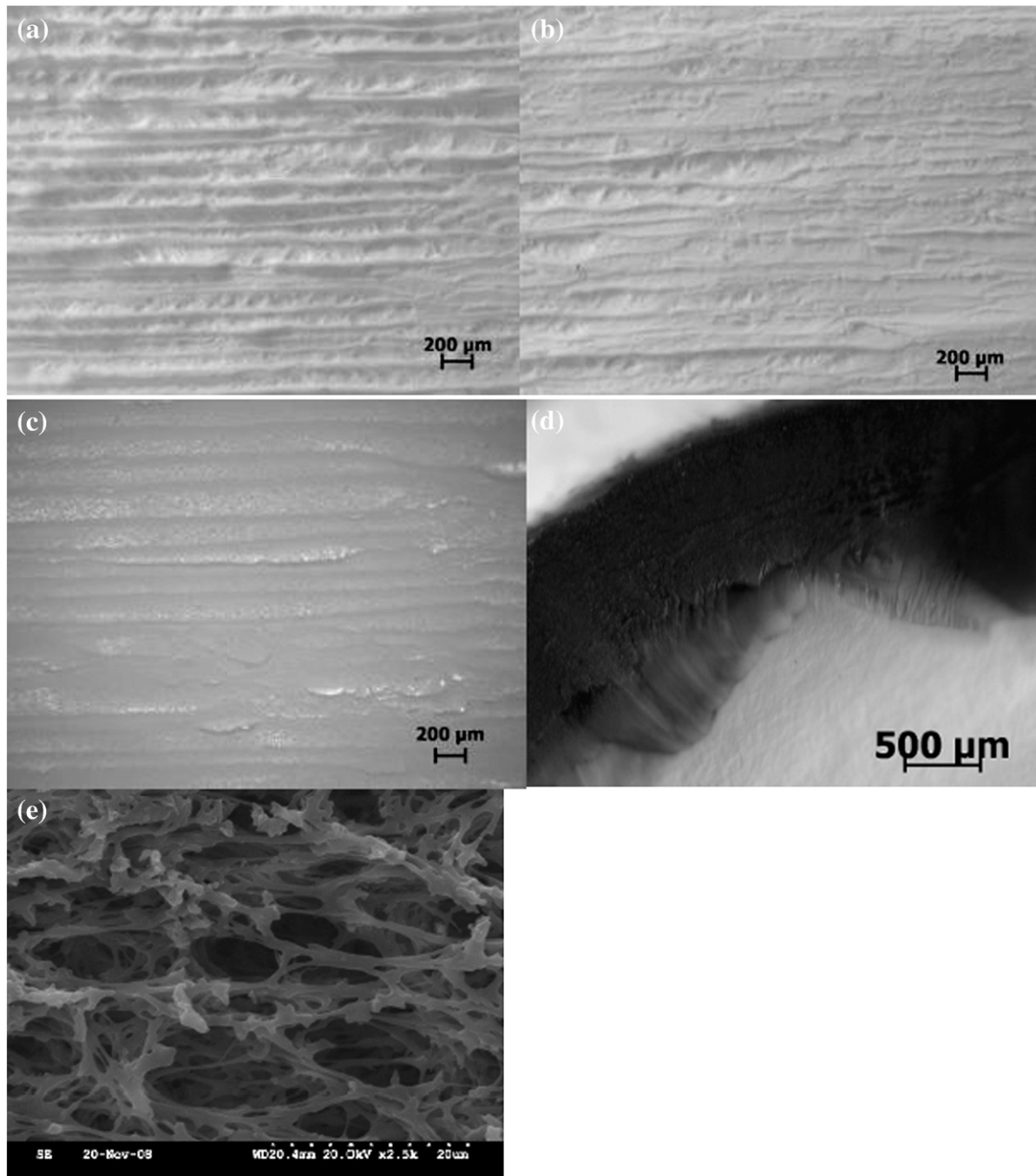
Fig. 8. Optical microscope images showing the dependence of groove size on the laser fluence at the sample scanning speed of 0.1 mm/s: (a) fluence = 5.7 J/cm^2 (b) fluence = 8.9 J/cm^2 (c) fluence = 11.5 J/cm^2 (d) fluence = 14 J/cm^2 (e) microstructure of the burned surface(SEM image).

The results of this set of experiments indicate that the surface quality is inversely proportional to the scanning speed as shown in Fig. 7, with the scanning speed decreasing and the pulse number increasing the cutting surface becomes smoother. However, when the sample scanning speed decreases to 0.02 mm/s, the total amount of absorbed energy is very high, which leads to a burned surface as shown in Fig. 7 (c). On the contrary, when the sample scanning speed is very fast, the material can't be completely melted and removed due to the less amount of energy absorbed, therefore the surface is rougher as shown in Fig. 7 (b). We found that the suitable sample scanning speed is 0.1–0.12 mm/s when the pulse energy is 6.3 J/cm^2.

In the next set of cutting experiments, the cutting surface was investigated as a function of pulse energy (fluence) in the range of
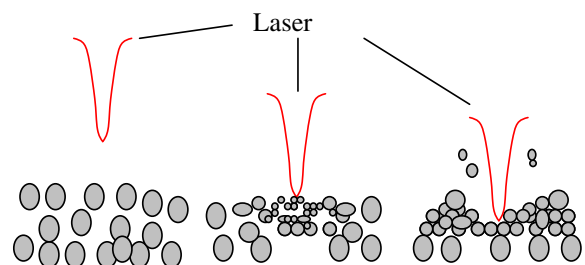

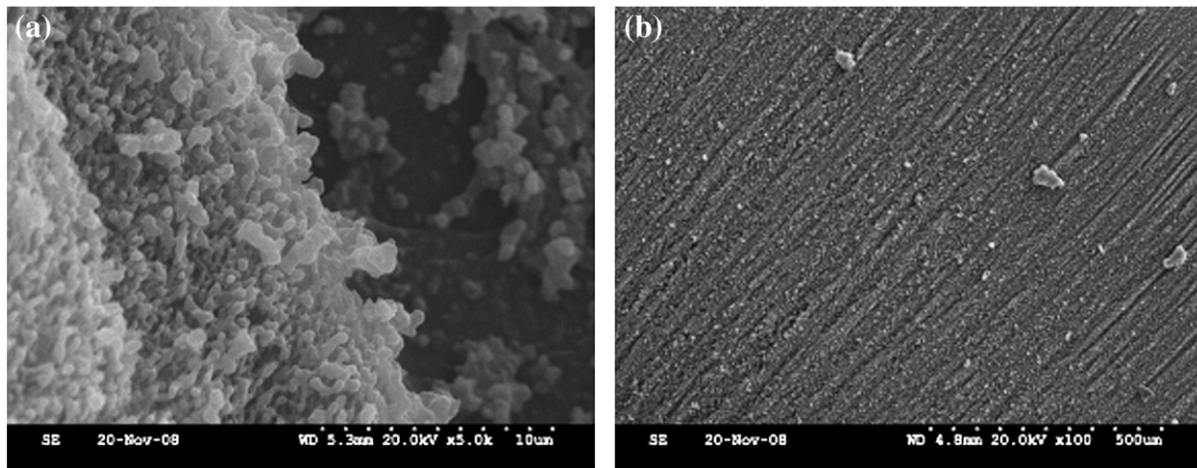**Fig. 9.** The schematic illustration of material removal mechanism.

Fig. 10. SEM images of ablated surface: (a) a groove peak and valley microstructure (b) surface showing ablation marks and particles.

$E_0 = 0.4$–1.2 mJ ($\varphi_0 = 5.1$–15 J/cm^2), at the sample scanning speed of 0.1 mm/s. The results are shown in Fig. 8 (a) (b) (c). The surface quality improves with the increasing beam fluence. However, if the fluence is increased to a critical value at certain scanning speed, e.g., 15 J/cm^2 at the scanning speed of 0.1 mm/s in our experiments, the heat is accumulated so much that the ablation surface is severely melted and burned as shown in Fig. 8 (d). The material is melted and recast into the weblike microstructure, as shown in Fig. 8 (e). The suitable energy (fluence) is found to be 0.5–0.7 mJ (6.3–8.9 J/cm^2) at the scanning speed of 0.1 mm/s for the linear scan and about 0.4–0.6 mJ (5.1–7.6 J/cm^2) at the scanning speed of 4° /s for the circular scan.

4. Discussion

Based on the investigations on the ablation rate and surface morphology of the polyurea aerogel using femtosecond laser pulses, we propose a femtosecond laser removal mechanism for the polyurea aerogel to help us better understand the machining results. Two main polymer ablation mechanisms have been reported and discussed for more than two decades: photochemical model and thermal/photo-thermal model. Both ablation models are based on the fact that the energy from laser pulse is initially transformed into electronic excitations [21]. Therefore, the ablation of polymers usually is a combination of photochemical and photothermal phenomenon. The role of each can be varying for different polymer materials and laser irradiation wavelengths [22]. Although the polyurea aerogel in our experiments has the unique porous structure, it is still a polymeric material. Therefore the material removal is realized through a combination of photothermal and photochemical mechanism. On the other hand, for the high laser intensity used in our experiments, it is believed that the polyurea aerogel ablation process is fundamentally initiated through multiphoton ionization.

Fig. 9 illustrates the proposed laser ablation mechanism for polyurea aerogel. When laser pulse irradiates the porous material, the photon energy is converted into heat because of the photothermal process. The material under the laser beam may be broken into smaller particles that become softened or even melted. The fluidic polymer fragments then flow away towards the two sides due to Gaussian beam energy distribution and surface tension. Some material fragments may be vaporized and ejected from the surface. In the end the material is redistributed due to the Gaussian beam energy distribution and the groove structure is formed as shown in Fig. 10 (a) (b). With the sample movement, a series of grooves are created by the complex interplay of overlapping beam paths. The amount of the beam path overlap determines the energy deposited on

a certain area. The more overlap, the more pulses and the more energy are deposited, and thus the smoother the formed surface. During the ablation process, the vaporized material may fall back on the newly formed surface as loose particles as shown in Fig. 10 (b).

The deposit energy density is the key factor to material removal as shown in our previous results. We can see that the cutting surface quality improves with the beam fluence as shown in Fig. 8. The groove width on the cutting surface increases with the beam fluence since more energy deposition causes more material to be melted. The result coincides with $\phi = \phi\sqrt{\ln(I/I_0)}$ [23], where ϕ_0 and I_0 are ablated groove width and laser intensity at ablation threshold and I and ϕ are applied laser intensity and the corresponding groove width. With the increase of intensity more energy is absorbed by the material and the material removal ability of the beam increases and surface quality is enhanced. In addition, the energy density on the material is determined by the sample scanning speed. As we discussed, the scanning speed can be converted to the pulse number due to the fixed beam diameter and the pulse repetition rate based on Eq. (2). The pulse number increases with the decrease of scanning speed. Both the pulse number and the pulse energy can affect the energy density deposited on the material. We can adjust the energy density deposited on the material by tuning the sample scanning speed (pulse number) and the laser pulse intensity. However, the energy density decreases
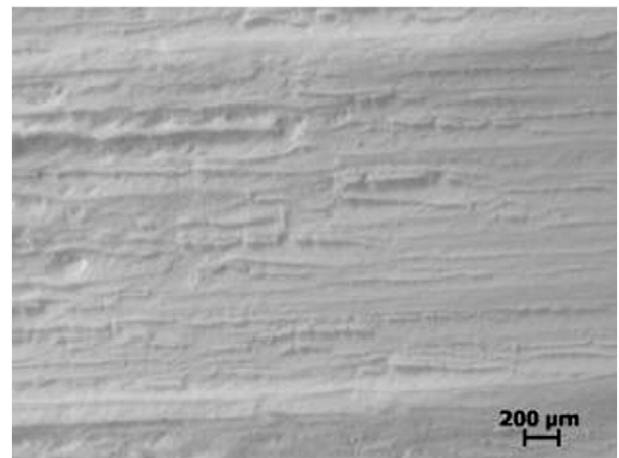

Fig. 11. Optical microscope image of the ablated surface at fluence of 8.9 J/cm^2 and scanning speed of 0.12 mm/s.
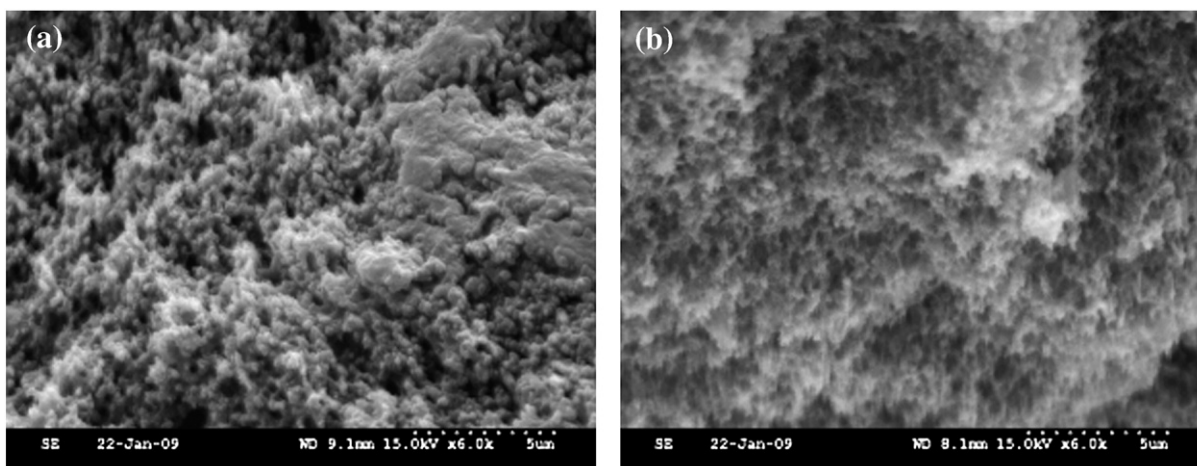
Fig. 12. SEM image of (a) the cross section 10 μm under the ablated surface (b) raw material.

with the beam propagation distance in the material because the laser light diffusely scatters in the porous material. When the pulse propagates to the exit side from the incident side, it gradually loses the material removal ability. Therefore, the surface roughness at the beam incident side is much better than at the beam exit side and this is reasonable since the pulse loses its ability to remove material after it propagates about 13 mm when the sample is linearly translated.

A similar surface quality may be achieved by different combinations of scanning speed and beam fluence to obtain the same energy density and thus the same surface quality. For example, we increased the pulse energy from 0.5 mJ (6.36 J/cm^2) to 0.7 mJ (8.9 J/cm^2) while raising the sample scanning speed from 0.05 mm/s to 0.12 mm/s to find that the surface morphology of the latter one is similar to the previous one, when comparing Fig. 7 (a) and Fig. 11. For both cases, the total energy density deposited on the material is about the same. Therefore, higher pulse energy implies that the ablation time can be shorter for the same amount of material removed, that is, the cutting efficiency is increased at the cost of the increased beam energy.

The formation of the rounded particulate microstructure, shown in Fig. 10 (a), also indicates that after the sample material absorbs enough energy from the laser pulse due to multiphoton absorption, it could decompose into small fragments and then melt into the rounded shape due to surface tension. The weak polymerization bond like C–O (3.6 eV), C=N (3.2 eV) and N–H (4.0 eV) are decomposed after multiphoton absorption, which is consistent with the previously reported model and mechanism [10,14,16,17].

Moreover, the porous microstructures are not destroyed by the laser pulse 10 μm beneath the ablation surface, as shown in Fig. 12 (a). From Fig. 12, we can see that the porous particulate structure after laser ablation is similar to the intact material. This is attributed to the ultra-short laser-material coupling time and the low thermal conductivity of the material [3]. However, the particle size appears to be larger after laser ablation.

5. Conclusions

Polyurea aerogel was successfully machined using femtosecond laser pulses. The material breakdown threshold is found to be 1.3 J/cm^2 at 800 nm center wavelength and 40 fs pulse width. The material ablation rate at different energy levels is found to be on the order of tens of microns per pulse. The periodic groovy surface structure after laser cutting is explained by a proposed material removal mechanism that includes material melting and vaporization. An important factor of this study is to determine the optimum regime of laser micromachining to create a high quality cutting surface by investi-

gating the influence of the key factors such as laser beam energy and sample scanning speed. The following parametric regime produces a high quality surface: the suitable beam fluence is 6.36–8.9 J/cm^2 while the sample is translated at the speed of 0.1–0.12 mm/s and 5.1–7.3 J/cm^2 while the sample is rotated at the speed of 3.5–4°/s. However, the surface quality is better with the beam circularly scanning the sample due to the reduced beam propagation distance. Based on the SEM image of the raw material and the ablated material we find that the porous microstructure remains the same at 10 μm under the ablation surface. Owing to femtosecond laser's high precision with negligible collateral damage, femtosecond laser pulses can be used to successfully cut highly porous polymer materials.

References

[1] USPTO Application #: 20060211840.
[2] K.E. Parmeter, F. Milstein, J. Non-Cryst. Solids 223 (1998) 179.
[3] J. Lee, G.L. Gould, W. Rhine, J. Sol-Gel Sci. Technol. 49 (2009) 209.
[4] M. Ali, T. Wagner, M. Shakoor, P.A. Molian, J. Laser Appl. 20 (2008) 169.
[5] J. Küger, W. Kautek, Adv. Polym. Sci. 168 (2004) 247.
[6] A.J. Lee, J.M. Dawes, M.J. Withford, J. Laser Appl. 20 (2008) 154.
[7] L. Ding, R.I. Blavkwell, J.F. Kunzler, W.H. Knox, Appl. Opt. 47 (2008) 3100.
[8] J. Sun, J.P. Longtin, P.M. Norr, J. Non-Cryst. Solids 281 (2001) 39.
[9] Z.B. Wang, M.H. Honga, J. Appl. Phys. 93 (2003) 6375.
[10] L.G. Reyna, Z.J. Watson, J. Appl. Phys. 78 (1995) 3423.
[11] J. Krüger, S. Martin, H. Mädebach, L. Urech, T. Lippert, A. Wokaun, W. Kautek, Appl. Surf. Sci. 247 (2005) 406.
[12] C.R. Mendonca, S. Orlando, G. Cosendey, M. Winkler, E. Mazur, Appl. Surf. Sci. 254 (2007) 1135.
[13] S. Juodkaz, V. Mizeik, S. Matsuo, K. Ueno, H. Mawa, Bull. Chem. Soc. Jpn 81 (2008) 411.
[14] T. Lippert, J.T. Dickinson, Appl. Surf. Sci. 127 (1998) 117.
[15] J.M. Liu, Opt. Lett. 7 (1982) 196.
[16] Y.S. Lee, X. Wen, W.A. Tolbert, D.D. Dlotta, M. Doxtader, D.R. Arnold, J. Appl. Phys. 72 (1992) 2440.
[17] P. Moreno, C. Me´ndez, A. Garc´ı a, I. Arias, L. Roso, Appl. Surf. Sci. 252 (2006) 4110.
[18] R. Gattass, E. Mazur, Nat. Photonics 2 (2008) 219.
[19] S. Mulik, C. Sotiriou-Leventis, N. Leventis, Chem. Mater. 20 (2008) 6985.
[20] S. Baudach, J. Bonse, J. Krüger, W. Kautek, Appl. Surf. Sci. 154 (2000) 555.
[21] T. Lipper, J. Dickinson, Chem. Rev. 103 (2003) 453.
[22] L. Urech, T. Lippert, C.R. Phipps, A. Wokaun, Appl. Surf. Sci. 253 (2007) 6409.
[23] S. Guizard, A. Semerok, J. Gaudin, M. Hashida, P. Martin, F. Queř, Appl. Surf. Sci. 186 (2002) 364.